Spin Effects on Spur Kinetics. 5. Modeling of Coherent Phenomena

Charlotte E. Bolton[†] and Nicholas J. B. Green*

Department of Chemistry, King's College London, Strand, London WC2R 2LS, U.K.

Received: October 27, 1998; In Final Form: February 1, 1999

We report an extension to our modified Monte Carlo simulation technique to model coherent spin effects (such as CIDEP) in spurs containing one or two pairs of neutral radicals under the influence of an applied magnetic field. The motivation for choosing such a system is to investigate whether it is possible to glean information about the initial distribution of the particles or the initial spin state of the spur from the simulated polarizations. An analysis of the system based upon the adiabatic approximation provides qualitative insight. However, further examination indicates that while it is possible to obtain explicit information about the initial spin state from the polarizations, the same does not appear to be true for the spatial configuration. The results for a two-pair spur are very different from those obtained for a single pair. To determine whether the two-pair polarizations can be explained in terms of pairwise interactions, and to mask the effects of averaging inherent in Monte Carlo simulations, single realizations of the spur evolution were performed. These indicate that at short times (<100 ps) the polarizations are induced in a complicated manner through the close proximity of all four particles, while at longer times successive two-body encounters are responsible.

1. Introduction

It has been established[1] that more than 70% of the energy lost from a fast charged particle to a condensed medium is localized in events of less than 100 eV. Each energy deposition event produces an isolated cluster ("spur") which typically comprises one or two ionization events and a similar number of excitation events.[2] The clusters therefore contain a small number of correlated ions, electrons, and neutral radicals, whose unpaired spins confer additional spin control on the diffusion-controlled reactions occurring in the spur.

In a typical radiolysis event the primary interaction with the fast electron ionizes the molecule and the secondary (slow) electron produced proceeds to ionize or excite further molecules in the vicinity. These secondary events are generally in close proximity to the primary event because the low-energy electron has a high inelastic cross section.

In the primary event the optical approximation is expected to be obeyed to a high degree of accuracy,[3] yielding a radical-ion pair in a singlet state. Regardless of the complexity of the secondary interactions, the overall spin state of the cluster of radicals produced must be conserved; thus, if $\Delta S = 0$ for the original event, the vector sum of all the spins in the spur must be zero at time zero.[4] During the secondary interactions exchange processes are likely to be important, leading to the production of triplet radical pairs, but these are always subject to the constraint that the spur is singlet-correlated overall. Our previous investigations[5−8] have shown that the chemistry of the radical reactions can be profoundly affected by the nature of these secondary interactions.

The role of spin in the kinetics of radiation tracks has been of interest for over 20 years,[9−11] while experimental manifestations of spin effects following irradiation, such as quantum beats in the recombination fluorescence[12,13] and polarizations (CIDEP) in radicals escaping recombination in the spur,[14,15] have also been reported.

Some theories have been proposed to explain and predict these spin effects,[16−19] but these are restricted to a single pair of radicals. The standard approach for investigating spin effects in photochemistry utilizes the stochastic Liouville equation (SLE[20]). Although the SLE can formally be extended to larger systems, the memory and storage requirements make this computationally unfeasible. Additionally, there are severe difficulties involved in the solution of many-body diffusion problems. It is clear that a generalized method capable of handling larger spurs is required for a complete description of the nonhomogeneous kinetics of a radiation track, since the multibody effects associated with the more densely ionized "track-ends"[21,22] are also known to be significant in the chemistry of irradiated systems. Low-energy (100−5000 eV) secondary electrons in low-LET tracks (e.g. from hard X-rays or γ-rays) account for 30−50% of the dose[23] and are primarily responsible for the lethality of such radiations in cellular systems.[24,25]

We have previously proposed[8] a method which has the potential to overcome the limitations of currently available theories. The technique is based upon a simultaneous random flights simulation of diffusive trajectories and integration of the time-dependent Schrödinger equation and is easily extended to spurs containing more than one radical pair.

The main purpose of the present paper is to report the extension of the random flights simulation technique to model polarizations in spurs containing more than one pair of radicals. The radical pair mechanism (RPM)[26,27] states that polarizations arise through the simultaneous operation of the exchange and Zeeman or hyperfine interactions. The simulation method has therefore been applied to systems of two radical pairs in an external magnetic field. This is a very complicated problem, and in order to keep the analysis manageable at this stage we have only included exchange and Zeeman interactions. Such a model is not totally unrealistic; there are experimental systems where coherent effects are dominated by the Zeeman interaction.[13] Inclusion of the hyperfine interaction introduces no new

[†] Present address: MRC Radiation and Genome Stabilty Unit, Harwell, Didcot, Oxon OX11 0RD, U.K.

10.1021/jp984212i CCC: $18.00
Published on Web 05/26/1999

methodological problems but makes interpretation of the results much more difficult and will be addressed in a future publication. Dipolar interactions may also be important in generating polarizations in radical-ion pairs[28] but have not been included in the model. Spin relaxation has also been excluded at this stage. The motivation for choosing such a system is to investigate whether any information about the initial distribution of radicals or their initial spin state can be gleaned from the polarizations. One of the major problems in radiation chemistry is that experimental kinetic data yield only a limited amount of information about the properties of the spur. It has been shown[29,30] that scavenging experiments basically contain the same information as the kinetic results. It is therefore hoped that coherent spin effects may provide additional insight into the initial spatial distributions and spin states.

The following section presents details of the random flights simulation method. Section 3 introduces our application of the SLE, which provides a stringent test for the simulation method and the results of the comparison for a single pair of radicals. The results of simulations for a system of two radical pairs are presented in section 4.

2. Monte Carlo Random Flights Simulation

The Monte Carlo random flights simulation method used to investigate coherent phenomena in spurs is essentially identical to that described in the previous paper.[8] Although the simulation technique has been described previously, a short résumé will be given here for the sake of completeness.

There are two parts to the simulation, namely the diffusive motion of the particles and their spin state. The diffusive trajectories of the particles are simulated using the normal Brownian dynamics approach of integrating a stochastic differential equation of the form[31,32]

$$\mathrm{d}\mathbf{R} = \frac{D\mathbf{F}}{k_\mathrm{B}T}\,\mathrm{d}t + \sqrt{(2D\,\mathrm{d}t)}\,\mathrm{d}\mathbf{W}_3 \qquad (1)$$

where **R** is the position vector, D is the diffusion coefficient, **F** is any force acting on the particle, dt is the time step, and d$\mathbf{W}_3$ represents the random Brownian force on the particle (three-dimensional white noise). In the absence of forces acting on the particles, the simulation uses the discretized form of eq 1, namely

$$\delta\mathbf{R} = \sqrt{(2\mathrm{D}\delta\mathrm{t})}N_3(0,1) \qquad (2)$$

where the variables are unchanged but the white noise is replaced by a 3-vector of normal random numbers of mean zero and variance one.[33] It is assumed that there are no spin-dependent effects on the diffusion process, in that the separation-dependent exchange interaction, $J(r)$, does not affect the relative diffusion (apart from reaction) and only operates when the particles approach to within ~1.0 nm. This assumption[34] is valid provided that $\hbar|J(r)| < k_\mathrm{B}T$, which holds for all interparticle separations attainable during the simulation.

The spin state of the radicals is incorporated into the simulation by integrating the time-dependent Schrödinger equation as the particles diffuse. The spin Hamiltonian for the system contains two terms: the exchange interaction, which depends on the particle configuration and is therefore constantly and randomly changing, and the Zeeman interaction with an external magnetic field, which is time-independent. The spin function is represented as a vector relative to a particular basis, and the spin Hamiltonian is then represented as a matrix. Several different bases are used in the course of the simulation.

The Hamiltonian for the Zeeman interaction with a magnetic field **B** is given by[35,36]

$$\hat{H}_z = \sum_i \mu_\mathrm{B} B\hat{S}_i = \sum_i g_i \mu_B B\hat{S}_{iz} \qquad (3)$$

where g_i is the g-factor for the interaction of spin $\hat{S}j$ with the magnetic field (**B**), which lies along the z-axis, S_{iz} is the projection of the spin onto the z-axis, and μ_B is the Bohr magneton. The Z-basis is the basis in which the Zeeman Hamiltonian matrix is diagonal; the basis functions are unambiguously labeled by a complete set of M_i and can therefore be represented $|\{M_i\}\rangle$. The diagonal elements of the Zeeman Hamiltonian are given by $\sum i g_i \mu_i B m_i$, where m_i is the magnetic quantum number.

The experimental phenomenon of CIDEP cannot occur without the exchange interaction, and therefore, the approximate model of "contact exchange" [9] is not sufficient for the purposes of modeling polarizations.

The exchange Hamiltonian is calculated from the expression[35,37,38]

$$H_\mathrm{ex} = \sum_{i>j} -J_{ij}(r_{ij})(2\hat{S}_i\hat{S}_j + {}^1/_2) = \sum_{i>j} -J_{ij}(r_{ij})[(\hat{S}_i^+\,\hat{S}_j^- + \hat{S}_i^-\,\hat{S}_j^+) + 2(\hat{S}_{iz}\hat{S}_{jz}) + {}^1/_2] \qquad (4)$$

where $\hat{S}_i$ and $\hat{S}_j$ are the electron spins on radical centers i and j, $\hat{S}^+$ and $\hat{S}^-$ are the shift operators for each electron spin, and $\hat{S}_{iz}$ and $\hat{S}_{jz}$ are the projections of each electron spin on the z-axis. Equation 4 assumes that the exchange interaction is dependent only upon the interparticle separation and is unaffected by the relative molecular orientations.[34,37−38] $J_{ij}(r_{ij})$ is then given by

$$J_{ij}(r_{ij}) = J_0 \mathrm{e}^{-\alpha(r_{ij}-R)} \qquad (5)$$

where J_0 is the exchange strength (typically −0.15 to −3.37 ps^{-1}),[39] α is the range parameter (typically 10.6−19 nm^{-1}),[39] r_{ij} is the interparticle separation, and R is the encounter distance (0.5 nm).

2.1. Method of Integration. The difficulty of integrating the Schrödinger equation arises because the exchange Hamiltonian depends on the particle configuration via the interparticle distances, which change randomly and continuously during the diffusive evolution of the spur. We have investigated several integration methods, ranging in complexity from a simple Euler-type discretization[40] to the diagonalization of the spin Hamiltonian at each time step. The nonzero time steps δt must be short enough to exclude three-body interactions and, more stringently, to allow the integral of the time-dependent Schrödinger equation to converge. The effect of changing the time step has been investigated to determine the longest time step possible without loss of accuracy; a value of 0.1 ps was used in the simulations reported here. Although the Euler-type discretization requires shorter time steps, it is more efficient at attaining a given level of accuracy than the more complicated diagonalization approach. Thus, at the end of each time step, the wave function is updated according to the simple linearization[35]

$$\phi(t+\delta t) = \psi(t) - i\delta t\hat{H}\phi(t) \qquad (6)$$

and then renormalized (since the linearization method does not conserve probability).

2.2. Basis Set. The speed of the simulation depends critically on the dimension of the spin space used. The previous paper in this series[8] described a method of reducing the size of the basis and associated operators and matrixes through the use of permutation group theory. The full spin space for a system of four radicals is 16-dimensional, but it is possible to reduce the dimension through the requirements of the conservation of spin.

In the absence of an external magnetic field, both S and M_s are conserved. Attention is limited to those basis functions with an M_s value of zero, since the spur is constrained to be overall singlet. The basis and operators are thus reduced to six dimensions. The basis functions in the Z-basis are $|\alpha\alpha\beta\beta\rangle$, $|\alpha\beta\alpha\beta\rangle$, $|\alpha\beta\beta\alpha\rangle$, $|\beta\alpha\alpha\beta>$, $|\beta\alpha\beta\alpha\rangle$, and $|\beta\beta\alpha\alpha\rangle$; however, in the absence of a field further reduction is possible because the spin Hamiltonian can be expressed in terms of symmetry elements of the S_4 permutation group. The representation spanned by the Z-basis can therefore be reduced in terms of S_4 irreducible representations (irreps). The symmetry-adaption indicates that the six $M_s = 0$ basis functions above span the irreps A_1, E, and T_1, which are one-, two- and three-dimensional, respectively, and correspond to the subspaces labeled by the spin quantum number of the spur, i.e., $S = 2$, $S = 0$, and $S = 1$, respectively.

If an external magnetic field is applied, the value of S is no longer conserved so this further reduction is not possible. However, it is still convenient to use the symmetry-adapted basis functions (hereafter denoted g), which are constructed from the Z-basis functions using projection operators for the appropriate irreps. Thus, the g-basis function spanning the one-dimensional A_1 irrep is totally symmetric. The choice of functions to span the $S = 0$ (two-dimensional) subspace is not unique, since there are three g-basis functions in which two pairs are singlet correlated. Each of these singlet vectors has a complementary vector (which is a combination of the other two) lying in the same space; the choice of orthogonal vector pair to span the $S = 0$ space is arbitrary and results in no loss of generality. The basis functions spanning the $S = 1$ (three-dimensional) subspace are mutually orthogonal and also orthogonal to the $S = 0$ and $S = 2$ basis functions.

The six basis functions, expressed as vectors in the Z-basis, are therefore the following:

$$g_1 = \frac{1}{\sqrt{6}}(\alpha\alpha\beta\beta + \alpha\beta\alpha\beta + \alpha\beta\beta\alpha + \beta\alpha\alpha\beta + \beta\alpha\beta\alpha + \beta\beta\alpha\alpha) = \frac{1}{\sqrt{6}}(1,1,1,1,1,1)$$

$$g_2 = \frac{1}{2}(\alpha\beta\alpha\beta - \alpha\beta\beta\alpha - \beta\alpha\alpha\beta + \beta\alpha\beta\alpha) = \frac{1}{2}(0,1,-1,-1,1,0)$$

$$g_3 = \frac{1}{\sqrt{12}}(2\alpha\alpha\beta\beta - \alpha\beta\alpha\beta - \alpha\beta\beta\alpha - \beta\alpha\alpha\beta - \beta\alpha\beta\alpha + 2\beta\beta\alpha\alpha) = \frac{1}{\sqrt{12}}(2,-1,-1,-1,-1,2)$$

$$g_4 = \frac{1}{\sqrt{2}}(\alpha\alpha\beta\beta - \beta\beta\alpha\alpha)\ \frac{1}{\sqrt{2}}(1,0,0,0,0,-1)$$

$$g_5 = \frac{1}{\sqrt{2}}(\alpha\beta\alpha\beta - \beta\alpha\beta\alpha) = \frac{1}{\sqrt{2}}(0,1,0,0,-1,0)$$

$$g_6 = \frac{1}{\sqrt{2}}(\alpha\beta\beta\alpha - \beta\alpha\alpha\beta) - \frac{1}{\sqrt{2}}(0,0,1,-1,0,0)$$

TABLE 1: Representation of the *S*-Basis Functions in Terms of the *g*- and *Z*-Basis Functions Defined Previously

S-function label	representation in *g*-basis	representation in *Z*-basis
$s(1) = S_a^{12}$	$\left(0,\frac{1}{\sqrt{2}},0,0,\frac{1}{2},\frac{1}{2}\right)$	$\frac{1}{\sqrt{2}}(0,1,0,-1,0,0)$
$s(2) = S_b^{12}$	$\left(0,\frac{-1}{\sqrt{2}},0,0,\frac{1}{2},\frac{1}{2}\right)$	$\frac{1}{\sqrt{2}}(0,0,1,0,-1,0)$
$s(3) = S_a^{13}$	$\left(0,\frac{1}{2\sqrt{2}},\frac{\sqrt{3}}{2\sqrt{2}},\frac{1}{2},0,\frac{1}{2}\right)$	$\frac{1}{\sqrt{2}}(1,0,0,-1,0,0)$
$s(4) = S_b^{13}$	$\left(0,\frac{-1}{2\sqrt{2}},\frac{\sqrt{-3}}{2\sqrt{2}},\frac{1}{2},0,\frac{1}{2}\right)$	$\frac{1}{\sqrt{2}}(0,0,1,0,0,-1)$
$s(5) = S_a^{14}$	$\left(0,\frac{-1}{2\sqrt{2}},\frac{\sqrt{3}}{2\sqrt{2}},\frac{1}{2},\frac{1}{2},0\right)$	$\frac{1}{\sqrt{2}}(1,0,0,0,-1,0)$
$s(6) = S_b^{14}$	$\left(0,\frac{1}{2\sqrt{2}},\frac{-\sqrt{3}}{2\sqrt{2}},\frac{1}{2},\frac{1}{2},0\right)$	$\frac{1}{\sqrt{2}}(0,1,0,0,0,-1)$
$s(7) = S_a^{23}$	$\left(0,\frac{-1}{2\sqrt{2}},\frac{\sqrt{3}}{2\sqrt{2}},\frac{1}{2},\frac{-1}{2},0\right)$	$\frac{1}{\sqrt{2}}(1,-1,0,0,0,0)$
$s(8) = S_b^{23}$	$\left(0,\frac{1}{2\sqrt{2}},\frac{-\sqrt{3}}{2\sqrt{2}},\frac{1}{2},\frac{-1}{2},0\right)$	$\frac{1}{\sqrt{2}}(0,0,0,0,1,-1)$
$s(9) = S_a^{24}$	$\left(0,\frac{1}{2\sqrt{2}},\frac{\sqrt{3}}{2\sqrt{2}},\frac{1}{2},0,\frac{-1}{2}\right)$	$\frac{1}{\sqrt{2}}(1,0,-1,0,0,0)$
$s(10) = S_b^{24}$	$\left(0,\frac{-1}{2\sqrt{2}},\frac{-\sqrt{3}}{2\sqrt{2}},\frac{1}{2},0,\frac{-1}{2}\right)$	$\frac{1}{\sqrt{2}}(0,0,0,1,0,-1)$
$s(11) = S_a^{34}$	$\left(0,\frac{1}{\sqrt{2}},0,0,\frac{1}{2},\frac{-1}{2}\right)$	$\frac{1}{\sqrt{2}}(0,1,-1,0,0,0)$
$s(12) = S_b^{34}$	$\left(0,\frac{-1}{\sqrt{2}},0,0,\frac{1}{2},\frac{-1}{2}\right)$	$\frac{1}{\sqrt{2}}(0,0,0,1,-1,0)$

In the simulation, the wave function is represented in the g-basis and is initially located in the $S = 0$ subspace (spanned by g_2 and g_3).

The exchange Hamiltonian can be expressed in terms of operations of the permutation group, but the same is not true of the Zeeman Hamiltonian because S is not conserved. The conservation of M_s and S by the exchange interaction and the mixing of S subspaces by the Zeeman interaction is apparent in the blocked forms of the Hamiltonian operators. The exchange Hamiltonian (in the g-basis) is of the form

$$\begin{pmatrix} a+b+c & 0 & 0 & 0 & 0 & 0 \\ 0 & 1/2(b+c)-a & -\sqrt{3}/2(b-c) & 0 & 0 & 0 \\ 0 & -\sqrt{3}/2(b-c) & 1/2(b+c)-a & 0 & 0 & 0 \\ 0 & 0 & 0 & a & c' & b' \\ 0 & 0 & 0 & c' & b & a' \\ 0 & 0 & 0 & b' & a' & c \end{pmatrix}$$

where $a = (J_{12} + J_{34})$, $a' = (J_{12} - J_{34})$, $b = (J_{13} + J_{24})$, $b' = (J_{13} - J_{24})$, $c = (J_{14} + J_{23})$, and $c' = (J_{14} - J_{23})$. Each S subspace is represented by a block in the Hamiltonian matrix.

In contrast to the exchange Hamiltonian, the six-dimensional Zeeman Hamiltonian (in the g-basis) is blocked on the opposite diagonal and mixes the spin subspaces:

$$\begin{pmatrix} 0 & 0 & 0 \\ 0 & 0 & 0 \\ 0 & 0 & 0 \\ 1/\sqrt{3}(++--) & 0 & 2/\sqrt{6}(++--) \\ 1/\sqrt{3}(+-+-) & 1/\sqrt{2}(+-+-) & -1/\sqrt{2}(+-+-) \\ 1/\sqrt{3}(+--+) & -1/\sqrt{2}(+--+) & -1/\sqrt{6}(+--+) \end{pmatrix}$$

$$\begin{pmatrix} 1/\sqrt{3}(++--) & 1/\sqrt{3}(+-+-) & 1/\sqrt{3}(+--+)\mathrm{T} \\ 0 & 1/\sqrt{2}(+-+-) & -1/\sqrt{2}(+--+) \\ 2/\sqrt{6}(++--) & -1/\sqrt{6}(+-+-) & -1/\sqrt{6}(+--+) \\ 0 & 0 & 0 \\ 0 & 0 & 0 \\ 0 & 0 & 0 \end{pmatrix}$$

The signs in the parentheses refer to the sign of the $g\mu_B\mathbf{B}$ factor for each electron in the spur.

2.3. Encounter and Reaction. The diffusive motion of the particles is modeled by the normal random flights method, and the Hamiltonians and wave function are updated at the end of each time step. At this point, it is also determined whether any pairs have encountered, either by proximity or via an interpolating bridging process[41,42] which allows for encounter and reseparation during the time step. The inner boundary is located at an interparticle separation of 0.5 nm; the probability of reaction at this separation is calculated by comparing a random number U (uniform on (0,1]) with the singlet probability of the encountering pair. To calculate this probability, the singlet part of the wave function must be projected out using the appropriate projection operator for the encountering pair. In the case of a singlet encounter, the wave function must be projected into the subspace in which the encounter pair is singlet. This subspace is two-dimensional since the wave function of the disjoint pair is spanned by the vectors $|\alpha\beta\rangle$ and $|\beta\alpha\rangle$, or, equivalently, $|S\rangle$ and $|T_0\rangle$. It is possible to define a set of 12 functions labeled S, of which there are 2 for each singlet-correlated encounter pair. The representation of these S-functions, in terms of the g-basis functions defined previously and in terms of the original Z-basis, is shown in Table 1. For example, the function $S_a{}^{14}$ describes a spin state in which the particles labeled "1" and "4" are singlet-correlated and the disjoint pair (particles "2" and "3") have spins α and β, respectively, while in $S_b{}^{14}$ the disjoint pair have spins β and α, respectively.

The projection operators are constructed from these S-functions by combining the outer products of each singlet-pair vector. Thus, $\hat{P}_{12} = (S_a{}^{12}(S_a{}^{12})^T + S_b{}^{12}(S_b{}^{12})^T)$. Once the nature of the encounter has been decided, the wave function is transformed by application of the projection operator and renormalized, effectively collapsing the wave function onto a pure singlet or triplet state. The reactive particles are removed from the system and their interactions zeroed. After a singlet encounter, the population of the $S = 2$ subspace is necessarily zero, since it is only possible to populate a quintet state if the system contains two triplet pairs. Thus, after a singlet encounter, the wave function for the remaining pair must remain in the $S = 0$ and $S = 1$ subspaces for the rest of its lifetime. To enforce this condition, the appropriate projection operator is reapplied to the wave function after it is updated at the end of each time step. This precaution ensures that rounding errors cannot repopulate the quintet subspace.

2.4. Calculation of Polarizations. Electronic polarizations are calculated from the wave function (in the Z-basis) at predefined times during the simulation, using

$$P = \sum_{j=1}^{2^n} m_{sj}|z_j|^2 \tag{7}$$

where n is the number of spins, m_{sj} is the magnetic spin quantum number of spin j, and z_j is the element of the wave function vector corresponding to spin j; the summation runs over all the radicals present.

3. Test of the Simulation Method: Stochastic Liouville Equation

In contrast to the Monte Carlo random flights simulation approach, the stochastic Liouville equation treats the system as an ensemble average and therefore requires a density matrix to be used[37,38,43] because of the loss of coherence between different realizations. The density matrix contains all possible information about the physical observables of the system, since its elements are quadratic combinations of the elements of the wave function vector,[44] z; i.e., $\rho_{ij} = \langle z_j{}^* z_i\rangle$. The SLE is an equation of motion for a generalized density matrix $\rho_{ij} = c(\mathrm{r})\langle z_j{}^* z_i|r\rangle$, where $c(r)$ is the probability density function of the configuration and the expectation is conditioned on the configuration.

The SLE simultaneously includes spin dynamics and interactions (via a spin Hamiltonian, $\hat{H}$) and the classical stochastic motion of the spin-carrying particles, represented by a diffusion operator, ∇^2. Details of spin-selective reaction, scavenging, relaxation, etc., may also be included.[37,38,43] The basic SLE is of the form

$$\frac{\partial\rho(r,t)}{\partial t} = D'\nabla^2\rho(r,t) + i[\rho(r,t),\hat{H}] \tag{8}$$

where D' is the relative diffusion coefficient for the radical pair.

Recognizing the spherical symmetry of the density matrix ρ and substituting $\rho = \sigma/r$ produces an equation of the form

$$\frac{\mathrm{d}\sigma}{\mathrm{d}t} = D\frac{\mathrm{d}^2\sigma}{\mathrm{d}r^2} + i[\sigma,\hat{H}] \tag{9}$$

which ignores any angular dependence in the exchange interaction and diffusive motion and is a function of the spatial variable r and the spins of the radical pair only.

The space is discretized, and a finite-difference method is employed to solve the SLE numerically in a standard way;[45] the Crank−Nicolson method[46] was chosen for its unconditional numerical stability.

All singlet-containing elements of the density matrix are set to zero at the inner boundary condition (at r = R), which is absorbing in nature. The element $|TT\rangle$ is reflected according to

$$\left.\frac{\partial\sigma}{\partial r}\right|_{r=R} - \frac{\sigma(R)}{R} = 0 \tag{10}$$

The spin part of the SLE depends on the Liouville operator, which is conventionally a commutator, constructed from the appropriate spin space for the system. For the simplest single-pair system, containing two electrons and no nuclei, the Zeeman basis is two-dimensional ($|\alpha\beta>$, $|\beta\alpha>$). The density matrix, which is 2×2, can then be represented as a four-dimensional vector, and the Liouville operator is represented as a 4×4 matrix, dependent on r through the exchange interaction $J(r)$. Since reaction is modeled using boundary conditions, these must be applied in the encounter ($S-T$) basis. It is therefore convenient to set up the whole numerical simulation of the SLE in this basis.

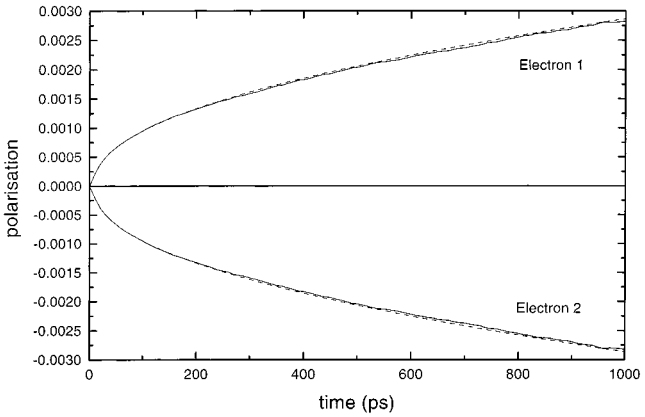

Figure 1. Comparison of the predicted polarizations from the random flights simulation and the SLE for a single pair initially in a singlet spin state. The magnetic field strength is 1.0 T, the initial separation is 1.0 nm, and $D' = 1.0 \times 10^{-8}$ m^2 s^{-1}. The polarizations are represented by the solid lines for the simulation and by the dashed lines for the SLE.

3.1. Results for a Single-Pair Spur. The SLE provides a stringent test of the Monte Carlo random flights technique for a single radical pair.

Figure 1 shows the electron polarizations for a spur containing two electron spins only. The particles are labeled "A" and "B" and have the characteristics of a hydrogen atom ($g_H = 2.002$) and hydroxyl radical ($g_{OH} = 2.024$) respectively but without the hyperfine interaction of the H atom or the spin relaxation of OH$^\bullet$. The hyperfine interaction and spin relaxation will be included in the model in the future. The system is sufficiently complex that, at the present time, the aim is to isolate coherent effects arising from the exchange and Zeeman interactions alone. The spur is initially in a singlet state, the initial separation of the pair is 1.0 nm, the relative diffusion coefficient is 1.0×10^{-8} m^2 s^{-1} ($D(A) = D(B) = 0.5 \times 10^{-8}$ m^2 s^{-1}), and the magnetic field strength is 1.0 T.

It is immediately obvious that there is very good agreement between the simulation results and the SLE calculation, suggesting that use of the random flights technique is justified.

Each SLE calculation takes approximately 10 min of CPU time on an IBM RS/6000 390H workstation and requires ~3 MB of memory. Although this memory requirement is well within the normal operating limits of the workstation, it should be pointed out that the system we are considering is a minimal basis set for a single radical pair. Increasing the size of the basis by including one nuclear spin increases the memory requirements to ~12 MB for a single calculation.

Polarizations are harder to obtain in Monte Carlo simulations than stochastic Liouville calculations because the Monte Carlo method considers one particular trajectory per realization, with many realizations required for the results to have statistical significance, whereas the stochastic Liouville calculation considers an ensemble average. This means that the simulation method is cpu-expensive. A typical simulation of 100 000 realizations for a radical pair with a minimal basis set takes ~ 10 h on an IBM RS/6000 390H workstation (and requires only ~ 300 kB of memory). However, simulation is the only option for systems where the SLE cannot be set up, e.g., two-pair spur or nondiffusive motion.

There are very large fluctuations in the polarizations from one realization to the next; frequently the standard deviation of the polarization can be 10 times larger than the expectation. Polarizations are usually very small, representing only a slight deviation from Boltzmann distributions. Polarizations arising from a single realization of the simulation may be far larger than those produced at the end of 10^5 independent realizations. The standard error for an average 10^5 realizations is typically ~3%, but the standard deviation for a single realization is 300 times larger than this.

4. Extension of the MCRF Simulation Method to a Two-Pair Spur

The simulation technique is readily extended in theory to model a two-pair spur. The main difficulty in modeling a larger system lies in the rapid increase in the dimensionality of the bases—the state space of a spur is 2^n-dimensional, where n is the number of spins in the spur. The associated increase in matrix size is reflected in the cpu-time required to simulate the spur.

We have used the extended simulation method to investigate the effects of changing various parameters on the modeled polarizations. The four particles in the spur are labeled "A" (particles 1 and 3) and "B" (particles 2 and 4) and, as for the single-pair system, have the same g-factors as in section 3.1. The particles are initially placed on the vertexes of a tetrahedron. In particular, we have investigated the effects of changing the initial size of the tetrahedron, the initial spin state of the spur, the diffusion coefficients of the particles, the exchange strength and range parameters, and the magnetic field strength. The coherent nature of CIDEP may suggest that the process by which polarizations develop is dependent solely upon the Zeeman interaction (and thus the external magnetic field). However, this is an oversimplistic view: it is the combination of the exchange interaction operating within each S subspace and the Zeeman interaction operating between S subspaces that generates polarizations. Removal of one or other of these interactions results in an unpolarized system. Increasing the strength of the magnetic field, the range of the exchange interaction, and the length of time spent at small separations all produce larger polarizations, while simulating the spur in the "contact exchange" (CE) limit[5] unsurprisingly does not produce polarizations at all.

The initial spin states for a two-pair spur can be expressed in terms of the basis functions $|SS\rangle$ and $(3)^{-1/2}(|T_{+1}T_{+1}\rangle - |T_0T_0\rangle + |T_{-1}T_{-1}\rangle)$.[6] These same spin states exist for any combination of radical pairs in the spur. If the spin correlations are between the pairs of radicals labeled 1−2 and 3−4, these spin states correspond to the basis functions g_2 ("sa") and g_3 ("ta"), respectively (see section 2.2).

Figure 2 shows the simulated polarizations of radicals escaping recombination for a two-pair spur initially in the "sa" spin state (A−B singlet-correlated pairs). The tetrahedron side length is 0.75 nm, while the relative diffusion coefficient is $D' = 1.0 \times 10^{-8}$ m^2 s^{-1}. The simulations have been performed at magnetic field strengths of 0.33 T (X-band) and 1.2 T (Q-band). It can easily be seen that increasing the magnetic field strength increases the magnitude of the polarizations. The product of the magnetic field and Δg determines the amount of singlet−triplet mixing, thus, a larger magnetic field causes a more rapid removal of the system from its initially unpolarized state into a superposition of spin states, some of which are preferentially populated (polarized). Encounters between particles with different g-factors (i.e. A−B encounters) are responsible for generating the polarizations, and the magnitude of the polarizations for each initial spin state is therefore correlated to some extent with the probability of the first encounter between an A−B radical pair being singlet in character. This point is illustrated in Figure 2 for the initial spin state "ta" (A−B triplet-

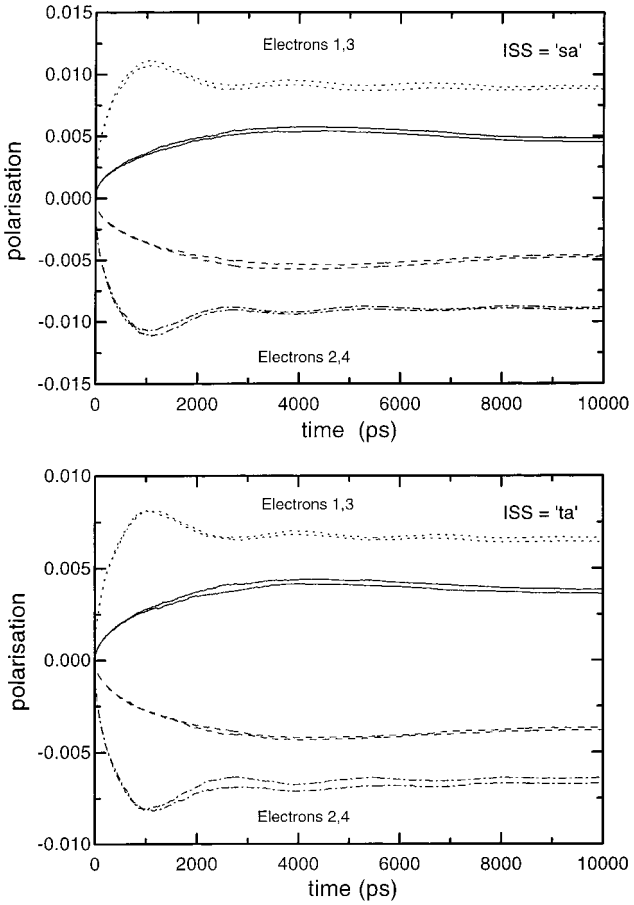

Figure 2. Comparison of the polarizations predicted by the random flights simulation for a two-pair spur initially in spin state "sa" (A−B singlets) and "ta" (A−B triplets). The particles are initially disposed on the vertexes of a tetrahedron of edge length 0.75 nm, and $D' = 1.0 \times 10^{-8}$ m^2 s^{-1}. The effect of changing the magnetic field strength on the polarizations is shown: the X-band (0.33 T) results are represented by the solid (electrons 1 and 3) and dashed (electrons 2 and 4) lines, while the Q-band (1.2 T) results are represented by the dotted (electrons 1 and 3) and dot−dashed (electrons 2 and 4) lines.

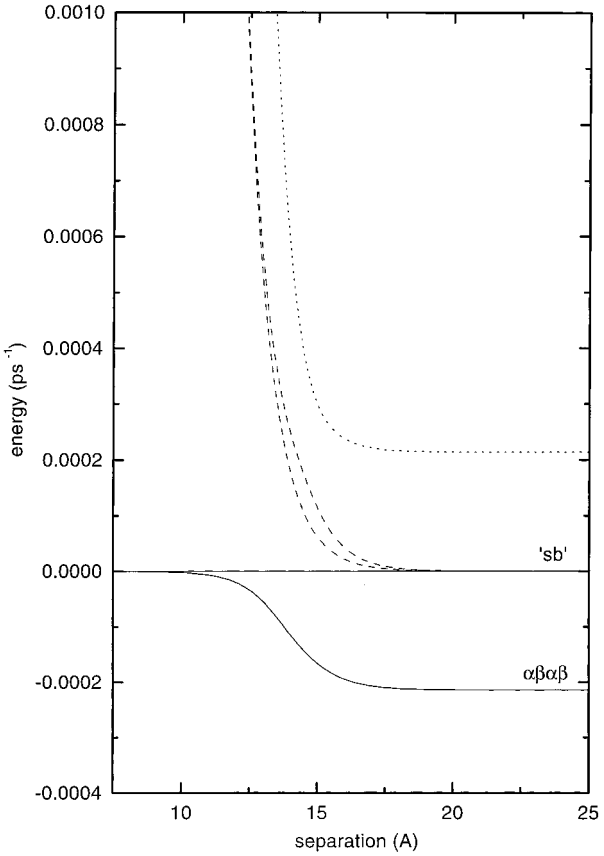

Figure 3. Correlation diagram in the adiabatic approximation for a tetrahedron distorted with tetrahedral symmetry, showing how a spin state initially located in the $S = 0$ subspace is correlated with the "sb" and $\alpha\beta\alpha\beta$ states at large separations. This enables the prediction of the sign of the polarization: positive for electrons 1 and 3; negative for electrons 2 and 4. The solid lines represent the $S = 0$ subspace, the dashed lines the $S = 1$ subspace, and the dotted line the $S = 2$ subspace.

correlated pairs), for which the A−B singlet encounter probability is smaller ($^3/_8$ vs $^5/_8$).[8] The correlation between the singlet encounter probability and the magnitude of the simulated polarizations is not exact, since the former applies solely to the first encounter.

The polarizations are observed to oscillate with a regular frequency under a magnetic field of 1.2 T. The period of the oscillations (∼3000 ps) is similar to the beat frequency ($\Delta g\mathbf{B}\mu_B$) in the Q-band. The maximum time of the simulations precludes the observation of similar oscillations under an X-band magnetic field. The oscillations appear in the ensemble average, but their origin is not clear, since they have not been observed in any single realizations.

At long times, the polarizations attain a steady level, and the sign of the polarization on a particular radical center is found to be the same in all systems under investigation (i.e. for all initial spin states, initial configurations, and diffusion coefficients). The adiabatic approximation has been applied to the system in order to predict the electron polarizations qualitatively. Of course, the simulation takes place in an adiabatic space since the spin state and the exchange interaction do not affect the relative diffusion of the particles, although the spin states themselves are treated nonadiabatically. Infinitely slow separation of particles initially disposed at the vertexes of a tetrahedron, so that the system remains in a stationary state at all times, allows the energy levels of each state to be plotted as a function of the particle separation. It is then possible to identify which states are likely to be occupied, given the initial spin state. The correlation diagram in Figure 3 indicates that from any initial spin state in the $S = 0$ subspace, the system is correlated with the $|\alpha\beta\alpha\beta>$ and (unpolarized) "sb" states at large separations. Although the adiabatic approximation is a gross simplification of the spur evolution, it does predict the sign of the polarization on each radical center correctly. The same correlation between the spin states is found if the tetrahedron is expanded symmetrically, with C_{3v} symmetry (faster expansion along one C_3 axis) or with D_{2d} symmetry (faster along one S_4 axis).

Decreasing the diffusion coefficient of the "B" particles to 2.8×10^{-9} m^2 s^{-1} produces larger polarizations (Figure 4), since the slower diffusion allows a longer period of exposure to the Zeeman and exchange interactions. The singlet and triplet subspaces are therefore mixed to a greater extent.

The trends exhibited in the previous figures are similar but less marked for systems where the initial interparticle separations are sampled from a Gaussian distribution of distances with $\sigma = 0.63$ nm, due to the increased separation between the particles and the averaging inherent in such a distribution. Figure 5 shows the simulated electron polarizations for systems initially in the "sa" and "ta" spin states at magnetic field strengths of 0.33 and 1.2 T, with $D' = 1.0 \times 10^{-8}$ m^2 s^{-1}.

If the initial wave function is a random superposition of basis functions from the $S = 0$ subspace, the simulated polarizations are intermediate in magnitude compared to the correlated spin

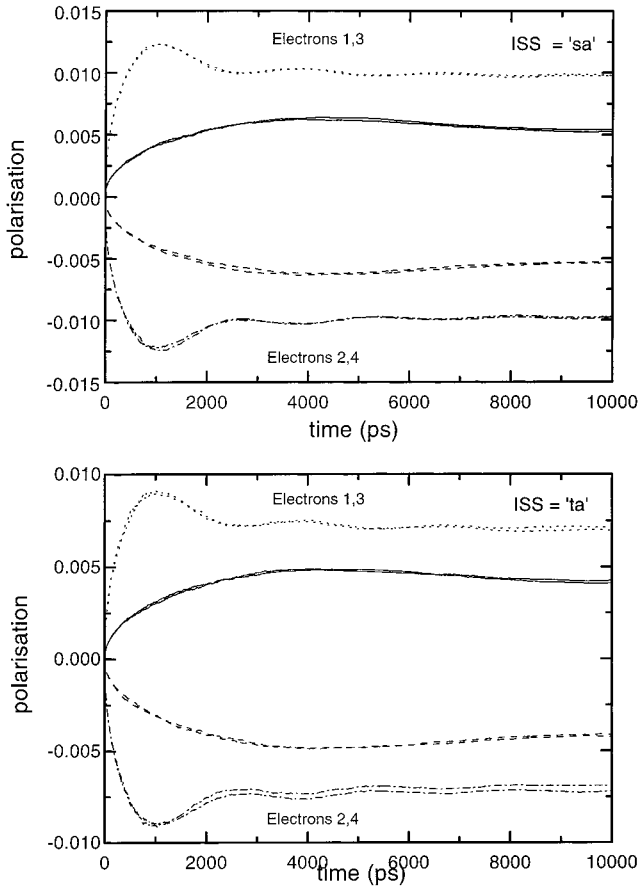

Figure 4. Comparison of the polarizations predicted by the random flights simulation for a two-pair spur initially in spin state "sa" (A−B singlets) and "ta" (A−B triplets). The particles are initially disposed on the vertexes of a tetrahedron of edge length 0.75 nm, and $D' = 0.78 \times 10^{-8}$ m^2 s^{-1}. The details are as for Figure 2.

states. This is not unexpected, since randomizing the spin state is equivalent to removing the spin correlations.

Figure 6 shows the long-time (at 10^4 ps) electron polarizations as a function of the angle theta (θ), where the initial wave function in the $S = 0$ subspace is given by $\Psi_0 = (\cos\theta, \sin\theta)$, where $\theta = 0°$ represents the spin state "sa" (A−B singlet-correlated radical pairs 1−2, 3−4), $\theta = 90°$ = "ta" (A−B triplet-correlated radical pairs 1−2, 3−4), $\theta = 60°$ = "sb" (A−A, B−B singlet-correlated radical pairs 1−3, 2−4), $\theta = 330°$ = "tb" (A−A, B−B triplet-correlated radical pairs 1−3, 2−4), $\theta = 120°$ = "sc" (A−B singlet-correlated radical pairs 1−4, 2−3), and $\theta = 30°$ = "tc" (A−B triplet-correlated radical pairs 1−4, 2−3). The trend is periodic and symmetric about each spin state, that is, the magnitudes of the polarizations for a particular spin state are identical (within the random error of the simulation) to those predicted for the same state differing only by a change of sign.

There is a large variation in the magnitude of the simulated polarizations with the initial spin state, whereby the polarizations predicted for the spin state "sb" are 40%−50% smaller than those for "tb". The largest polarizations are found when the A + B reaction yield is highest, since they are generated by an A−B pair after the first pair has reacted. An A−A or B−B encounter tends to kill any polarization that has developed on the radicals of the encountering pair; the pair may be equally and oppositely polarized on the radical centers, but this produces a total polarization for each species (A or B) of zero. If an A−B pair is polarized, however, the individual polarizations will not cancel each other out, so that the total polarization for each species is not zero but identical to the individual values.

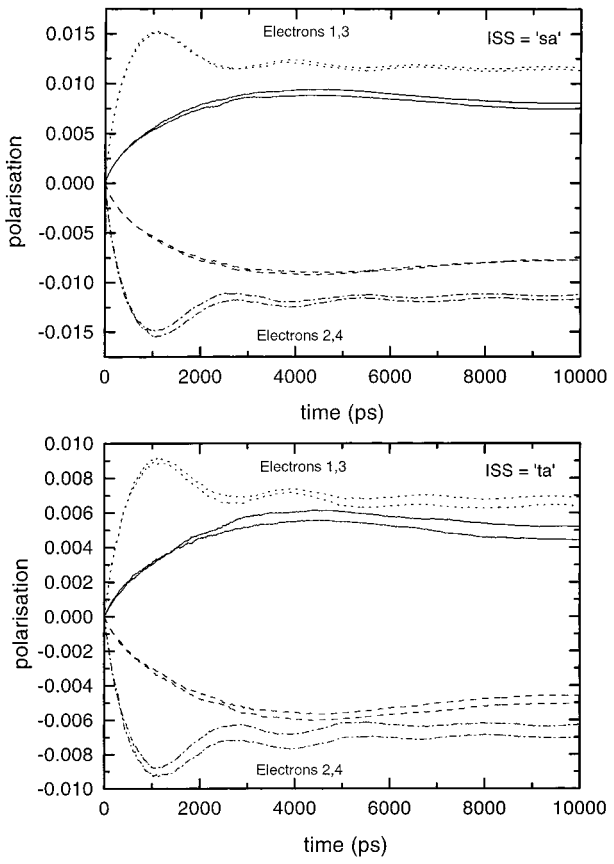

Figure 5. Comparison of the polarizations predicted by the random flights simulation for a two-pair spur initially in spin state "sa" (A−B singlets) and "ta" (A−B triplets). The particles are initially located at the vertexes of a tetrahedron of edge length 0.75 nm with the positions approximated by Gaussian distributions of $\sigma = 0.63$ nm, and $D' = 1.0 \times 10^{-8}$ m^2 s^{-1}. Details are as for Figure 2.

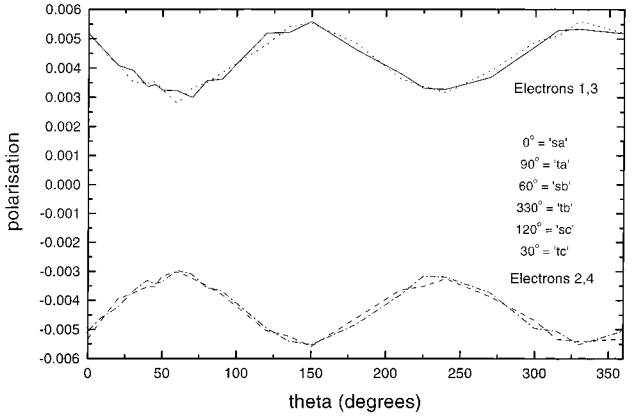

Figure 6. Variation of the electron polarizations predicted by the random flights simulation as a function of the angle θ. The initial wave function (in the $S = 0$ subspace) is given by $\psi_0 = (\cos\theta, \sin\theta)$, where $\theta = 0°$ represents the spin state "sa" (A−B singlet-correlated radical pairs 1−2, 3−4), $\theta = 90°$ = "ta" (A−B triplet-correlated radical pairs 1−2, 3−4), $\theta = 60°$ = "sb" (A−A, B−B singlet-correlated radical pairs 1−3, 2−4), $\theta = 330°$ = "tb" (A−A, B−B triplet-correlated radical pairs 1−3, 2−4), $\theta = 120°$ = "sc" (A−B singlet-correlated radical pairs 1−4, 2−3), and $\theta = 30°$ = "tc" (A−B triplet-correlated radical pairs 1−4, 2−3). The magnetic field strength is 0.33 T, and $D' = 1.0 \times 10^{-8}$ m^2 s^{-1}. The solid lines represent the polarization on electron 1, the dashed lines those for electron 2, the dotted lines those for electron 3, and the dot−dashed lines those for electron 4.

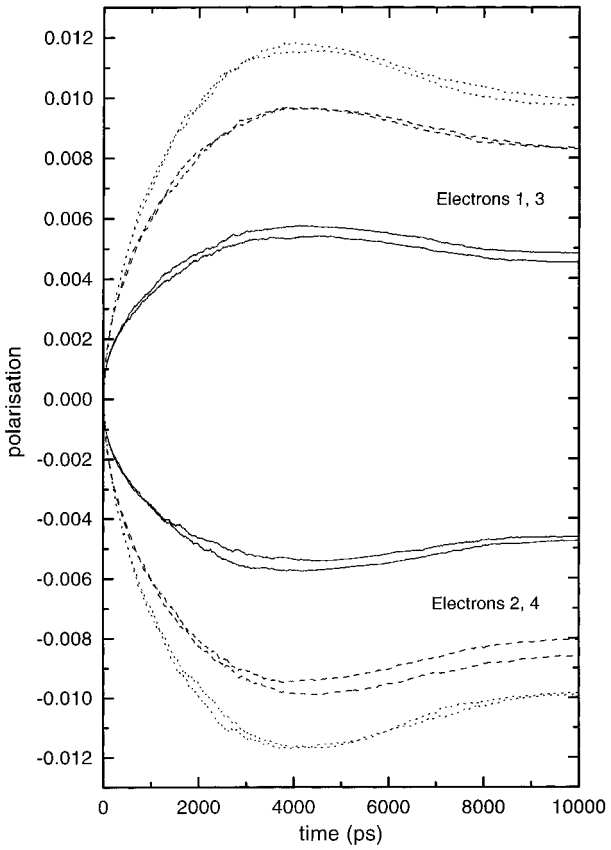

Figure 7. Comparison of the polarizations predicted by the random flights simulation for a two-pair spur initially in spin state "sa" (A−B singlets). The particles are initially disposed at the vertexes of tetrahedra of edge length 0.75, 1.2, and 1.65 nm, the magnetic field strength is 0.33 T, and $D' = 1.0 \times 10^{-8}$ m^2 s^{-1}. The solid lines represent the electron polarizations predicted for $r_0 = 0.75$ nm, the dashed lines the polarizations for $r_0 = 12$ nm, and the dotted lines those for $r_0 = 1.65$ nm.

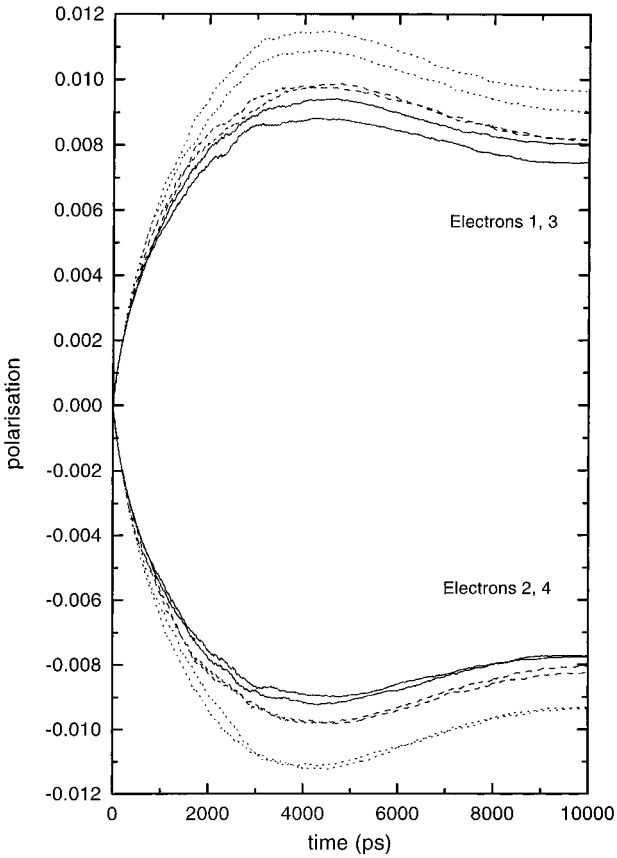

Figure 8. Comparison of the polarizations predicted by the random flights simulation for a two-pair spur initially in spin state "sa" (A−B singlets). The particles are initially located at the vertexes of tetrahedra of edge length 0.75, 1.2, and 1.65 nm with the positions approximated by Gaussian distributions of $\sigma = 0.63$ nm. The magnetic field strength is 0.33 T, and $D' = 1.0 \times 10^{-8}$ m^2 s^{-1}. The details are as for Figure 7.

It can be concluded from the results presented above that it is possible to derive information about the initial spin state of the system from the simulated polarizations. By changing the size of the initial tetrahedron, we have investigated whether it is also possible to draw conclusions about the initial spatial distribution of the particles. Figure 7 shows the simulated polarizations for a system initially in the "sa" spin state, under a magnetic field of 0.33 T, at initial tetrahedron sizes of 0.75, 1.2, and 1.65 nm. These distances were chosen to vary the relative magnitudes of the exchange and Zeeman interactions. At a separation of 0.75 nm, the exchange interaction between a radical pair predominates over the Zeeman interaction, while the reverse is true when the particles are much further (1.65 nm) apart. The intermediate value of 1.2 nm was chosen as the separation at which the exchange and Zeeman interactions are of comparable strength. At first sight it appears that the magnitude of the polarizations does reflect the initial distribution. However, normalizing the polarizations to the number of surviving particles in the system seems to remove this effect. The same conclusion applies if $D' = 0.78 \times 10^{-8}$ m^2 s^{-1} ("B" particles diffuse more slowly) and with a larger magnetic field (Q-band, 1.2 T). The results for a system with the particle positions sampled from a Gaussian distribution ($\sigma = 0.63$ nm), shown in Figure 8, provide even stronger evidence against the original premise, as might be expected. Unfortunately, it does not seem possible to derive spatial information from the simulated polarizations in a manner similar to the spin information.

Another important point arising from these results is that the simulated polarizations for a two-pair spur are very different to those obtained in a single-pair system. To investigate whether the polarizations in a two-pair system could be explained in terms of pairwise interactions, or if more complicated multibody effects were involved, we ran a series of single realizations of the spur evolution. The simulated polarizations in an individual trajectory may be far larger than those produced by averaging 10^5 independent realizations. The polarizations may also have the "wrong" sign according to the adiabatic approximation, which is not expected to be accurate under conditions of prolonged exposure to the exchange and Zeeman interactions and repeated reencounters. A single realization for a two-pair spur initially in the "sa" spin state is shown in Figure 9. The magnetic field strength was 1.2 T and $D' = 1.0 \times 10^{-8}$ m^2 s^{-1}. The upper plot represents the polarizations while the lower plot illustrates the interparticle separations for the reactive and disjoint pairs. This allows changes in the polarizations to be identified with specific encounters. At short times, polarizations are induced in a complicated way on all particles in close proximity. Close encounters during which the exchange interaction is operating allow polarizations to develop, while collisions destroy the polarizations of the encountering pair. In Figure 9, the first reaction (B + B, between particles 2 and 4) occurs extremely quickly at ~1.8 ps, at which time some of the negative polarization on these particles is transferred to the slightly positively polarized particle 3, with a concurrent change in the polarization on particle 1. The disjoint pair are less than 1.0 nm away from the reacting pair when the reaction occurs.

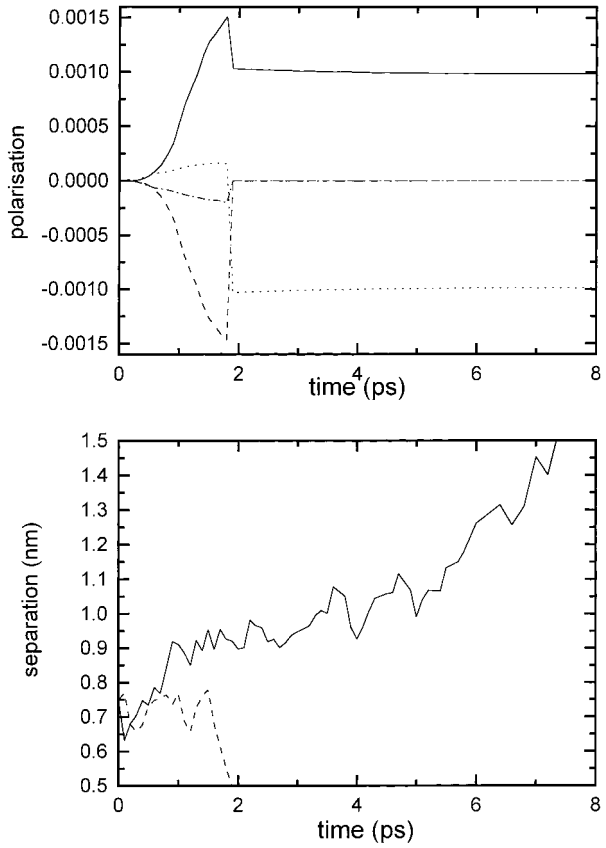

Figure 9. Single realization of the simulated spur evolution for a two-pair spur initially in an "sa" spin state (A−B singlets). The magnetic field strength is 1.2 T, and $D' = 1.0 \times 10^{-8}$ m^2 s^{-1}. The upper plot depicts the simulated polarizations, with the solid line representing electron 1, the dashed line electron 2, the dotted line electron 3, and the dot−dashed line electron 4. The lower plot depicts the interparticle distances for the reacting pair (electrons 1 and 3; solid line) and the disjoint pair (electrons 2 and 4; dashed line).

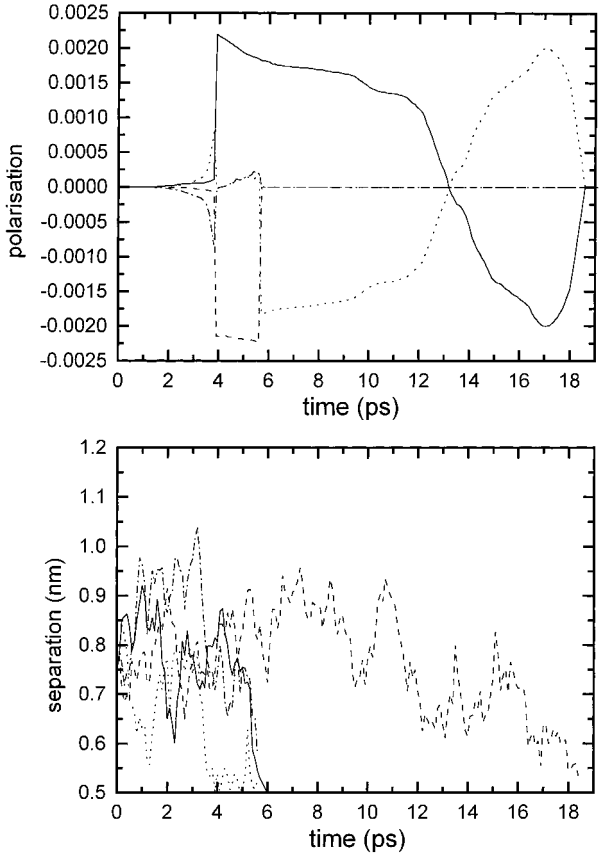

Figure 10. Single realization of the simulated spur evolution for a two-pair spur initially in an "sb" spin state (A−A, B−B singlets). The magnetic field strength is 1.2 T, and $D' = 1.0 \times 10^{-8}$ m^2 s^{-1}. The upper plot depicts the simulated polarizations, with the solid line representing electron 1, the dashed line electron 2, the dotted line electron 3, and the dot−dashed line electron 4. The lower plot depicts the interparticle distances for the reacting pair (electrons 1 and 3; solid line), the disjoint pair (electrons 2 and 4; dashed line), the 3−4 pair (dotted line), and the 2−3 pair (dot−dashed line).

Subsequently, the polarization on the remaining particles is steady, equal and opposite, since the particles are separating and have $\Delta g = 0$. The particles diffuse back into close proximity (<1.0 nm) at ∼80 ps and ∼500 ps (not shown), as a result of which the polarizations are reversed and then increase in magnitude.

In the radical pair mechanism, the Zeeman mechanism cannot produce polarizations for an identical pair of radicals, since Δg is zero. However, Figure 10 clearly shows that the polarizations of a single A−A pair remaining after a reaction can be altered by an encounter. This behavior is possible for a pair whose wave function is a superposition of $|S\rangle$ and $|T_0\rangle$ states, since the coefficients of $|\alpha\beta\rangle$ and $|\beta\alpha\rangle$ are different. Under these conditions, the polarizations change under the influence of the exchange interaction. Figure 10 illustrates this phenomenon for a system initially in an "sb" spin state (A−A, B−B singlet pairs), with $D' = 1.0 \times 10^{-8}$ m^2 s^{-1} and a magnetic field of 1.2 T. The polarizations on particles 1 and 3 evolve in a regular and symmetric manner following the earlier reaction between particles 2 and 4 (at ∼6 ps). At early times, four-body effects are responsible for the growth in polarization on all particles. Repeated triplet encounters produce almost identical positive polarization on particles 3 and 4 during their prolonged proximity. The negative polarization on particle 2 then appears to be transferred to particle 3 when the reaction between particles 2 and 4 occurs. A further close (∼0.65 nm) encounter of the remaining pair at ∼13 ps reverses the sign of the polarization on each center, before they react ∼5 ps later. The total polarization for each species is zero after the first (B + B) reaction, since the polarization on the remaining A particles is equal and opposite.

The effect of particular encounters on the *total* polarization for each species is shown in Figure 11, again for a single realization of a system initially in the "sb" spin state with $D' = 1.0 \times 10^{-8}$ m^2 s^{-1} and a magnetic field of 1.2 T. The development of polarization at short times (<40 ps) can be attributed initially to the close proximity of the 1−2 (A−B) pair, with a sharp increase as the other A−B pair diffuses together and then reacts (at ∼45 ps). At the point of reaction, the polarizations on the reacting particles are transferred to the disjoint pair, changing the sign of the polarization on these radicals in the process. Subsequently, the system remains polarized by the 1−2 pair, whose individual polarizations have the "wrong" sign according to the adiabatic approximation. This pair diffuses back to a separation where the exchange interaction begins to dominate (<1.0 nm), which reverses the sign of the polarizations.

An important point to note is the effect of exposure to the Zeeman and exchange interactions on the magnitude of the simulated polarizations. An extremely rapid reaction (cf. Figures 9, 10, and 12) allows insufficient time for the generation of large polarizations, which are consequently 10 or 20 times smaller than those predicted in Figure 11.

Figure 12 illustrates the generation of polarizations from multibody effects at very short times, when the particles are in

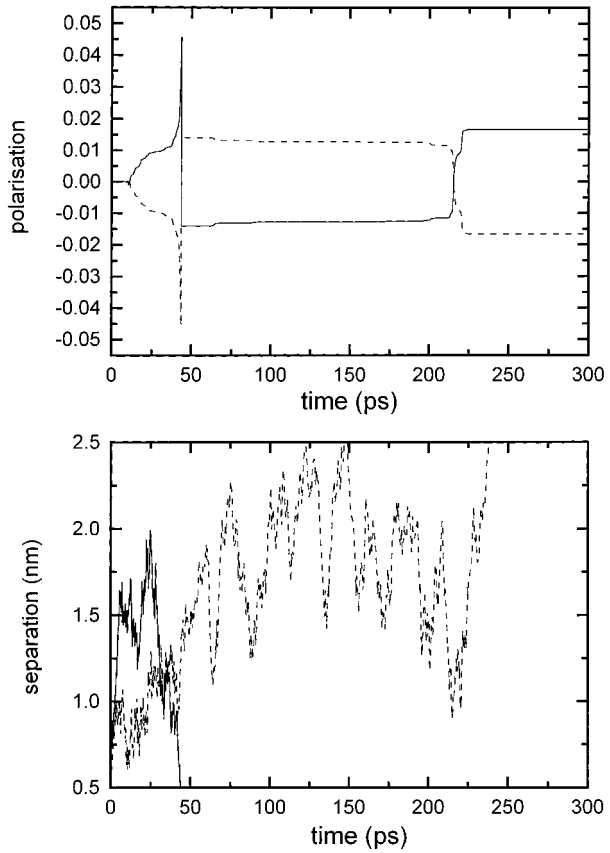

Figure 11. Single realization of the simulated spur evolution for a two-pair spur initially in an "sb" spin state (A−A, B−B singlets). The magnetic field strength is 1.2 T, and $D' = 1.0 \times 10^{-8}$ m^2 s^{-1}. The upper plot depicts the simulated polarizations, with the solid line representing the total polarization for electrons 1 and 3 and the dashed line the total polarization for electrons 2 and 4. The lower plot depicts the interparticle distances for the reacting pair (electrons 3 and 4; solid line) and the disjoint pair (electrons 1 and 2; dashed line).

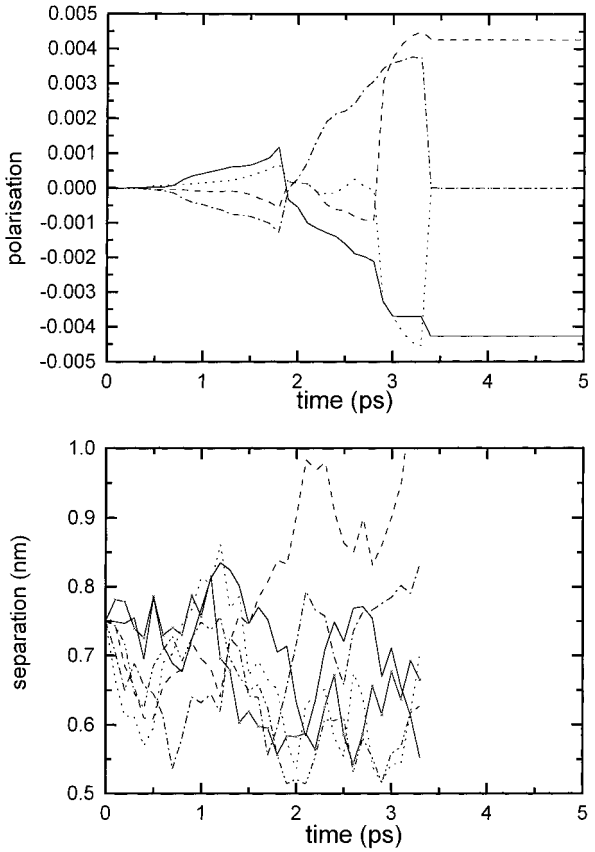

Figure 12. Single realization of the simulated spur evolution for a two-pair spur initially in an "sb" spin state (A−A, B−B singlets). The magnetic field strength is 1.2 T, and $D' = 1.0 \times 10^{-8}$ m^2 s^{-1}. The upper plot depicts the simulated polarizations, with the solid line representing electron 1, the dashed line electron 2, the dotted line electron 3, and the dot−dashed line electron 4. The lower plot depicts the interparticle distances for each of the pairs of electrons: reacting pair (electrons 3 and 4; solid line); disjoint pair (electrons 1 and 2; dashed line); 1−3 pair (dotted line); 1−4 pair (dot−dashed line); 2−3 pair (double-dot−dashed line); 2−4 pair (the solid-crossed line).

very close proximity. The system is initially in a "ta" spin state (A−B triplet-correlated pairs), at a magnetic field strength of 1.2 T and with $D' = 1.0 \times 10^{-8}$ m^2 s^{-1}. Prior to the (A + B) reaction between particles 3 and 4 at ∼3.5 ps, all four radicals are within 1.0 nm of each other and, thus, interacting predominantly via the exchange reaction. Unreactive encounters at ∼2 and ∼2.8 ps causing abrupt changes in the polarizations could be attributable to any of the radical pairs, none of which are sufficiently distant to be disregarded.

In conclusion, we have applied our modified Monte Carlo simulation technique to a variety of idealized systems containing two spin-correlated pairs of radicals in an attempt to determine what information about the initial state of the spur can be obtained from electron polarizations. While it does seem possible to derive information about the initial spin state of the spur, there seems to be no information about the particle distributions.

Additionally, we conclude that it is not sufficient to analyze multipair spurs solely in terms of pairwise interactions. The value of M_s is conserved throughout the evolution of the spur: if polarizations on encountering radicals are not equal and opposite, their polarization is transferred onto the remaining radicals (the disjoint pair), since the polarizations always sum to zero. Changes in the simulated polarizations at longer times occur mainly in discrete two-body encounters (after the first rapid reaction has occurred). Multibody effects can therefore be analyzed in terms of successive two-body encounters, although the whole spin state must always be considered. However, at short times polarizations arise as a result of the close proximity of all four particles and must be described properly using the trajectories of all the radicals.

Acknowledgment. This research was supported by the EPSRC under Grant Number GR/J71212. C.E.B. also thanks the EPSRC for a research studentship. The authors also acknowledge helpful discussions with Dr. P. J. Hore (Physical and Theoretical Chemistry Laboratory, University of Oxford).

References and Notes

(1) Pimblott, S. M.; LaVerne, J. A.; Mozumder, A.; Green, N. J. B. *J. Phys. Chem.* **1990**, *94*, 488.
(2) Pimblott, S. M.; Mozumder, A. *J. Phys. Chem.* **1991**, *95*, 7291.
(3) Platzman, R. L. *Vortex* **1962**, *23*, 282.
(4) Brocklehurst, B. *Int. Rev. Phys. Chem.* **1985**, *4*, 279.
(5) Green, N. J. B.; Pimblott, S. M.; Brocklehurst, B. *J. Chem. Soc., Faraday Trans.* **1991**, *87*, 2427.
(6) Pimblott, S. M.; Green, N. J. B.; Brocklehurst, B. *J. Chem. Soc., Faraday Trans.* **1991**, *87*, 3601.
(7) Green, N. J. B.; Pimblott, S. M.; Brocklehurst, B. *J. Chem. Soc., Faraday Trans.* **1995**, *91*, 223.
(8) Bolton, C. E.; Green, N. J. B. *J. Phys. Chem.* **1996**, *100*, 8807.
(9) Brocklehurst, B.; Higashimura, T. *J. Phys. Chem.* **1974**, *78*, 309.
(10) Magee, J. L.; Huang, J.-T. J. *J. Phys. Chem.* **1972**, *76*, 3801.
(11) Magee, J. L.; Huang, J.-T. J. *J. Phys. Chem.***1974**, *78*, 310.
(12) Anisimov, O. A.; Bizyaev, V. L.; Lukzen, N. N.; Grigoryantz, V. M.; Molin, Yu. N. *Chem. Phys. Lett.* **1983**, *101*, 131.

(13) Veselov, A. V.; Melekhov, V. I.; Anisimov, O. A.; Molin, Yu. N. *Chem. Phys. Lett.* **1987**, *136*, 263.
(14) Bartels, D. M.; Craw, M. T.; Han, P.; Trifunac, A. D. *J. Phys. Chem.* **1989**, *93*, 2412.
(15) Bartels, D. M.; Chiu, T. M.; Trifunac, A. D.; Lawler, R. G. *Chem. Phys. Lett.* **1986**, *123*, 497.
(16) Salikhov, K. M.; Molin, Yu. N.; Sagdeev, R. Z.; Buchachenko, A. L. *Spin Polarisation and Magnetic Effects in Radical Reactions*; Elsevier: Amsterdam, 1984.
(17) Molin, Yu. N.; Sagdeev, R. Z.; Salikhov, K. M. In *Soviet Scientific Reviews Section B (Chemistry Reviews)*; Vol'pin, M. E., Ed.; Harwood Academic Publishers: London, 1979.
(18) Muus, L. T., Atkins, P. W., MacLauchlan, K. A., Pedersen, J. B., Eds. *Chemically Induced Magnetic Polarisation*; Reidel: Dordrecht, The Netherlands, 1977.
(19) Lepley, A. R.; Closs, G. L. Eds. *Chemically Induced Dynamic Nuclear Polarisation*; Wiley-Interscience: New York, 1973.
(20) Kubo, R. *J. Math. Phys.* **1963**, *4*, 174.
(21) Green, N. J. B.; Harris, R. *Chem. Phys. Lett.* **1992**, *198*, 81.
(22) Pimblott, S. M.; Alexander, C.; Green, N. J. B.; Burns, W. G. *J. Chem. Soc., Faraday Trans.* **1992**, *88*, 925.
(23) Nikjoo, H.; Goodhead, D. T. *Phys. Med. Biol.* **1991**, *36*, 229.
(24) Goodhead, D. T.; Nikjoo, H. *Int. J. Radiat. Biol.* **1989**, *55*, 513.
(25) Goodhead, D. T.; Brenner, D. J. *Phys. Med. Biol.* **1983**, *28*, 485.
(26) Kaptein, R.; Oosterhoff, L. J. *Chem. Phys. Lett.* **1969**, *4*, 195; **1969**, *4*, 214.
(27) Closs, G. L. *J. Am. Chem. Soc.* **1969**, *91*, 4552.
(28) Shkrob, I. A. *Chem. Phys. Lett.* **1996**, *264*, 417.
(29) Green, N. J. B.; Pimblott, S. M. *Mol. Phys.* **1991**, *7*, 811.
(30) Pimblott, S. M.; LaVerne, J. A. *Radiat. Prot. Dosim.* **1994**, *52*, 183.
(31) Arnold, L. *Stochastic Differential Equations*; Wiley: New York, 1972.
(32) Gikhman, I. I.; Skorokhod, A. V. *Stochastic Differential Equations*; Springer: Berlin, 1971.
(33) Green, N. J. B.; Pilling, M. J.; Pimblott, S. M. *Radiat. Phys. Chem.* **1989**, *34*, 105.
(34) Pedersen, J. B.; Freed, J. H. *J. Chem. Phys.* **1974**, *61*, 1517.
(35) Landau, L. D.; Lifshitz, E. M. *Quantum Mechanics (Non-Relativistic Theory)*; Pergamon: Oxford, U.K., 1977.
(36) Atkins, P. W. *Molecular Quantum Mechanics* Oxford University Press: Oxford, U.K., 1983.
(37) Pedersen, J. B.; Freed, J. H. *J. Chem. Phys.* **1973**, *58*, 2746.
(38) Pedersen, J. B.; Freed, J. H. *J. Chem. Phys.* **1973**, *59*, 2869−2885.
(39) de Kanter, F. J. J.; Hollander, T. A.; Huizer, A. H.; Kaptein, R. *Mol. Phys.* **1977**, *34*, 857.
(40) Brocklehurst, B. *Faraday Discuss. Chem. Soc.* **1984**, *78*, 303.
(41) Clifford, P.; Green, N. J. B. *Mol. Phys.* **1986**, *57*, 123.
(42) Green, N. J. B. *Mol. Phys.* **1988**, *65*, 1399.
(43) Evans, G. T.; Fleming, P. D., III; Lawler, R. G. *J. Chem. Phys.* **1973**, *58*, 2071.
(44) ter Haar, D. *Rep. Prog. Phys.* **1961**, *24*, 304.
(45) Smith, G. D. *Numerical Solution of Partial Differential Equations: Finite Difference Methods*; Oxford University Press: Oxford, U.K., 1985.
(46) Crank, J.; Nicolson, P. *Proc. Camb. Philos. Soc.* **1947**, *43*, 50.